

Training Hybrid Deep Quantum Neural Network for Reinforcement Learning Efficiently

Jie Luo^{1*} and Xueyin Chen^{2†}

^{1*} Anyon Computing Inc., 4000 Harland Street, Emeryville, 94608,
California, USA.

² Los Angeles, 90035, California, USA.

*Corresponding author(s). E-mail(s): jluo@anyoncomputing.com;

†These authors contributed equally to this work.

Abstract

Quantum computing offers a new paradigm for computation, exploiting an exponentially growing Hilbert space for data representation and operation. Results are obtained from sampling over qubit state distributions that can have complex correlations from entanglement produced by the quantum computing process. Quantum machine learning (QML) emerged recently as a novel interdisciplinary research direction, developing novel machine learning architectures with quantum blocks. While large-scale fault-tolerant quantum machines are not yet available, recent works on hybrid QML models, compatible with noisy intermediate-scale quantum computers, have hinted at improved performance. Such hybrid deep quantum neural networks (hDQNNs) integrate GPU/CPU-based deep neural networks (DNNs) with parameterized quantum circuits (PQC) that can be straightforwardly executed on quantum processors. However, efficiently training hDQNNs using quantum hardware compatible batch backpropagation through PQCs was unavailable, limiting hDQNNs' scalability and usefulness for complex modern machine-learning tasks. Here, we present a scalable QML architecture that overcomes these challenges and demonstrates efficient batch optimization through PQC blocks to update associated model DNNs, enabling scalable hDQNN training compatible with physical quantum computers. Applied to the high-dimensional complex reinforcement learning benchmark, Humanoid-v4, successfully for the first time, our method highlights that hDQNN can deliver improved performance over models based on widely used state-of-the-art classical architectures. These findings offer a pathway toward leveraging near-term hybrid quantum-classical (hQC) computing systems for large-scale machine learning and underscore the potential of hQC architectures in advancing reinforcement learning and artificial intelligence.

Keywords: Quantum Computing, Machine Learning

1 Introduction

Quantum computing has initially attracted significant attention for its potential to solve classically challenging problems by exploiting data representation and operation in a Hilbert space that grows exponentially with the number of qubits [1]. Machine learning (ML) is an application field that could benefit greatly from quantum computing as increasingly large datasets and embedding dimensions challenge the limits of conventional computing hardware and more data efficient methods are necessary for advancing artificial intelligence with the depletion of available Internet data for training [2]. Quantum machine learning (QML) aims to harness quantum effects, such as superposition and entanglement, to enhance the efficiency and generalizability of learning beyond classical methods. Although fault-tolerant quantum machines—capable of running complex circuits without error—are not yet available to exponentially accelerate computing [3], the rapid development of noisy intermediate-scale quantum (NISQ) devices has inspired a new class of QML techniques designed to operate under NISQ constraints [1].

Reinforcement learning (RL) is the cornerstone of artificial intelligence (AI) [4]. Learning to generate classical distributions that model the patterns in data is critical for realizing RL models with high performance. This has been seen in the state-of-the-art (SOTA) AI and continuous variable control models utilizing stochastic learning architectures such as OpenAI PPO [5], SAC [6], and DeepSeek GRPO [7]. Recent quantum supremacy experiments [8–10] experimentally demonstrated NISQ quantum devices’ ability to generate distributions where measured qubit states exhibit complex correlations. Such distributions can be challenging for classical methods to efficiently simulate with the same amount of classical resources (compute and memory). NISQ quantum systems’ unique ability to generate nontrivial distribution in sampled output data has the potential to better model complicated correlations in stochastic real-world problems [6], achieving higher evaluation rewards, data efficiency, and robustness. Recent work [11] has shown that SOTA quantum reinforcement learning (QRL) with PPO modified to incorporate parametrized quantum circuits (PQCs), could have similar performance as the classical baseline models [12] on simple reinforcement learning benchmarks [13]. This hybrid quantum machine learning is realized as a hybrid deep quantum neural network (hDQNN). Here, the deep neural networks (DNNs) are used to encode input data into their outputs, which are then passed as control parameters to their connected PQCs in forward inference flow, seeking to leverage the quantum circuits’ high-dimensional Hilbert space as feature embedding spaces and low-dimensional classical inputs and outputs as bottleneck layers [14, 15]. QRL potentially excels in very complex high-dimensional reinforcement learning tasks. However, a significant barrier for applying hDQNNs to such complex high-dimensional problems is the cost of backpropagating through the PQC to update associated classical DNNs that generate input for it. Although methods exist for estimating gradients of a given forward

quantum circuit [1], these can be inefficient in practice, especially for real quantum hardware, when the input and output dimensions are large because $I \times O$ different circuits are required to estimate all the gradients of a PQC with I input dimensions and O output dimensions and each circuit needs a number, S , of shots to have the statistics for estimating the observables used to calculate gradients. Moreover, learning for complex problems with a high sample data efficiency [6] would require training data to be sampled from past experiences in a batch of size N_b for each DNN update with batch optimization. Furthermore, physical quantum hardware cannot easily support parallelization for handling the backpropagation in parallel. Therefore, existing QML methods that directly estimate gradients of the PQC are faced with a prohibitive practical overhead proportional to $I \times O \times S \times N_b$ for running on real quantum hardware. For example, in the case of using a fast superconducting Josephson junction quantum processor that has gate time as short as 20 ns and measurement time in the range of 100 ns [9, 10], a 10-layer 10-qubit PQC would need $I = 220$ and $O = 10$ with $N_b = 256$ and $S = 1000$ in our example for learning complex Humanoid-v4 environment. In this case, each update to model DNN parameters would require about 281.6 s. Considering that typical classical RL training even for simple tasks would likely require $\sim 10^6$ [6] update steps, this would translate to more than 10 years of training. In the context of reinforcement learning [5], this means current QRL methods are not scalable. The lack of high-throughput training strategies compatible with NISQ hardware limits practical performance and applicability to real-world machine-learning tasks.

In this work, we introduce a solution that enables efficient batch optimization for hDQNN at scale. This allows applying hDQNNs to learning complex high-dimensional tasks. We demonstrate the approach on challenging Humanoid-v4 reinforcement learning benchmark with better performance over widely adopted classical SOTA counterparts. This report is organized as follows. We will introduce the QML architecture that enables scalable training of hDQNN with classical DNNs interleaved with PQCs in Sec. 2. Following this, Sec. 3 will extend the scalable hDQNN architecture for reinforcement learning tasks and show the experimental results demonstrating that our hDQNN outperforms comparable classical methods as well as publicly reported models using SOTA RL architectures such as PPO [5], SAC [6], and TD3 [16]. In the last Sec. 4, we will discuss novel features observed in experiments and outlooks to train significantly larger models.

2 Neural PQC Tangential Approximation

Modern machine learning methods are established with highly efficient backpropagation-based training. Backpropagation utilizes well-known chain rules for vector calculus to infer the contribution of each learnable parameter (weights and biases) of a DNN in the loss function value by reversely traversing the computation graph of the DNN from the loss. This proven learning method relies on each computing operation node in the DNN’s computation graph to have a closed-form analytical expression for its gradients that can be explicitly predefined and efficiently calculated (in parallel) during training. The backpropagated loss mapped back from the final loss through the chain of gradients on the computation graph are used to update the

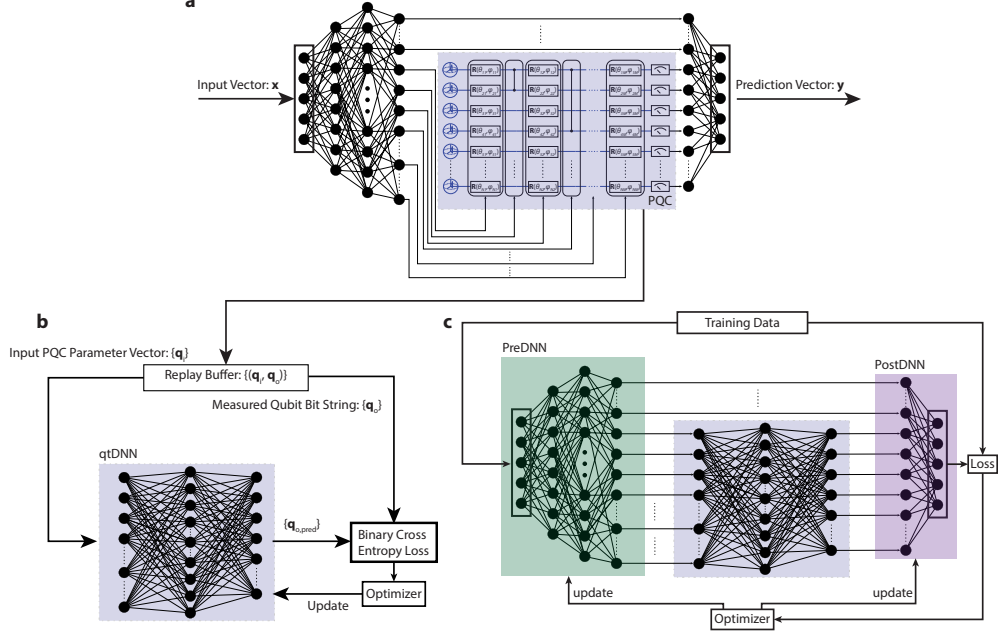


Fig. 1 **a**, a typical hybrid deep quantum neural network (hDQNN) contains a PreDNN connected to a PostDNN via both d_{c-link} direct connections and a quantum layer realized as a parametrized quantum circuit. The hDQNN enumerates the training dataset and records $(\mathbf{x}, \mathbf{y}_{pred}, \mathbf{y}, \mathbf{q}_i, \mathbf{q}_o)$ of each forward process into a buffer \mathcal{M} . In an update epoch, a batch of N_b entries is sampled from \mathcal{M} for updating hDQNN parameters. **b**, $\{(\mathbf{q}_i, \mathbf{q}_o)\}$ from \mathcal{M} is stored into a qtDNN Replay Buffer. N_{qt} tiny-batches, $\{\mathcal{B}_{qt}\}$, are sampled from \mathcal{B} are then used to update qtDNN towards approximating PQC in \mathcal{B} . **c**, the updated qtDNN is then used in the surrogate model Q_{qt} in this update step to facilitate the batched backpropagation of loss that are used to update the PreDNN and PostDNN with fixed qtDNN.

network parameters such that the updated network could have decreased difference between the model's predictions and targets in the training dataset. This learning process repeats until the final loss reaches below an acceptable value prescribed by the developer or arrives at a steady state. On the other hand, hDQNNs are typically developed using PQCs to act as functional layers without learnable parameters. They connect data and neural layers (NL) in a model, as seen in Fig. 1a. In these cases, PQCs can be called quantum layers (QL). The classical DNNs before and after the QL are respectively called PreDNN and PostDNN in this work. d_{c-link} classical links directly connecting PreDNN and PostDNN are added. These direct links allow classical communication between the DNNs around a QL. Information forwarded from the PreDNN through the classical links could help the PostDNN properly handle the QL's sampled outputs. For these QLs with a given parametrization structure, the input vector to the QL contains elements that are PQCs' controlling parameters used in defining the quantum gates to be executed. The QL output vector (sampled bistring)'s elements are the (most probable) measurement results of qubits. Note that qubit measurement results are intrinsically stochastic. This is because a QL maps its

input data into a high-dimensional Hilbert space spanned by all possible observable qubit states (bitstrings) as basis vectors. Therefore, for a QL containing N -qubits, the embedding space is 2^N -dimensional. Measurements on the embedded data effectively project the data onto one of the basis states with a probability depending on the weight of the basis state in the original state vector. Consequently, obtaining a QL’s output vector is equivalent to sampling the underlying probability distribution generated by the PQC. QLs convert inputs non-trivially into probability distributions of bitstrings and outputs are sampled from them. This fundamentally differentiates QLs from traditional functional layers with deterministic mappings from inputs to outputs or traditional sampling layer where the reparameterization trick [6] on parametrized normal distribution can be used.

It is challenging to backpropagate loss efficiently through QLs as reparameterization trick is not applicable to QLs. Various strategies have been developed in recent years [1]. Most widely used methods obtain the gradient vector of a PQC with respect to its input parameters by varying each input parameter and using repeated PQC executions to estimate its partial derivative with respect to each varied input. Such methods become quickly intractable as the input and output dimensions become large. Despite requiring many repeated measurements that scale with the size of input and output, methods based on direct PQC gradient estimation are intrinsically unfeasible to batch backpropagate loss in parallel, prohibiting efficient batched training for a hDQNN at scale, especially when it is applied to complex reinforcement learning.

This section presents a hDQNN architecture that is scalable for training while allowing QLs executable on physical quantum computers to be interleaved between classical DNNs. As mentioned, quantum layers are incompatible with efficient batched loss backpropagation for training the DNNs in the hDQNN model. Even though the fundamental physics of quantum layers executed on a quantum computer offer a new route to potentially more generalizable models utilizing nontrivial correlation between nodes related to entanglement between qubits, while, at the same time, hindering training hDQNN efficiently, we propose the quantum tangential space learning architecture that moving approximates the local behaviors of a QL with a classical DNN (qtDNN). For each hDQNN update step with a batch of training data sampled from the training dataset, qtDNN is trained as a local approximation to the QL within the batch, as illustrated in Fig. 1b. This provides scalability through classical batched backpropagation and retains the ability to develop more generalizable machine learning models incorporating QLs running on NISQ computers, overcoming the unique trade-offs.

In contrast to standard practice of designing machine learning models that emphasize avoiding over-fitting the training data, qtDNNs are not negatively impacted by overfitting. Instead, the most resource-efficient is training qtDNN to be an moving local first-order approximation of the target PQC’s behaviors local to each sampled data batch (mini-batch) for updating the hDQNN. qtDNN facilitates batch optimization as differentiating and backpropagating through classical DNNs are scalable and established. Therefore, a qtDNN bridges backpropagated loss at the output of its corresponding QL to the classical PreDNN. To make training a qtDNN more efficient, we add a replay buffer (qtDNN-buffer) to each QL that stores the input, \mathbf{q}_i , and sampled

output, \mathbf{q}_o , of the quantum layer as a pair, $(\mathbf{q}_i, \mathbf{q}_o)$, from each given batch of training data. This qtDNN-buffer is then used to train the qtDNN repeatedly with N_{qt} tiny-batches randomly sampled from this qtDNN-buffer. This qtDNN-buffer improves the qtDNN training data efficiency and accelerates qtDNN’s convergence to a moving approximation to its target quantum layer locally in the batch of data for updating hDQNN. Moreover, as the qtDNN aims to approximate the expected bitstring from sampling a target quantum layer, we utilize the binary cross entropy (BCE) loss function to train qtDNN.

The training process for hDQNN with qtDNN can be separated into the forward exploration, in Fig. 1a, and update epoch with two stages as in Fig. 1b and c. To be explicit, we denote the original hDQNN with quantum layers as a function $Q : \mathbb{R}^n \rightarrow \mathbb{R}^m$ where n and m are the dimensions of model input and output, respectively. We further define the training surrogate network approximating Q as $Q_{qt} : \mathbb{R}^n \rightarrow \mathbb{R}^m$. Q_{qt} always shares Q ’s classical model DNNs and replaces quantum layers with qtDNNs. We further define the training data containing input and target pairs as (\mathbf{x}, \mathbf{y}) and training Q is updating its DNNs’ parameters such that $Q(\mathbf{x}) \simeq \mathbf{y}$.

In the forward exploration process, input \mathbf{x} from the training data is passed through Q one at a time. In this process, a memory buffer \mathcal{M} storing the input \mathbf{x} , output \mathbf{y}_{pred} , target \mathbf{y} , and PQC’s \mathbf{q}_i and \mathbf{q}_o is populated. As this exploration process continues populating the \mathcal{M} with sufficient entries, the update epoch can start by sampling a batch, \mathcal{B} , of N_b entries from \mathbf{x} . In the first step of the epoch shown as Fig. 1b, qtDNNs are updated N_{qt} times with N_{qt} tiny-batches $\{\mathcal{B}_{qt}\}$ of data sampled from \mathcal{B} , to approximate the responses of Qs local to \mathcal{B} . In the following update step shown as Fig. 1c, the parameters (e.g., weights and biases) of all model DNNs shared by Q and Q_{qt} are updated with \mathcal{B} . In this parameter updating step, qtDNNs are not updated as they are fixed for \mathcal{B} by the previous step.

3 Quantum Reinforcement Learning

The qtDNN-architecture can be readily applied to solve reinforcement learning (RL) problems with hDQNN. This section shows a typical RL framework utilizing hDQNN with qtDNN-architecture as illustrated in Fig. 2 and Table. 1. We further implement this hDQNN with qtDNN architecture to solve a complex continuous variable reinforcement learning problem, Humanoid-v4 [13], and demonstrate excellent performance reaching a high final episode reward of 6011 in test compared to models reported on HuggingFace utilizing widely adopted classical state-of-the-art (SOTA) architectures such as PPO (episode reward = 685.21) [17], SAC (episode reward = 5742.10) [18], and TD3 (episode reward = 5306.47) [19]. We note that original works [5, 6] proposing PPO and SAC only carried out experiments on early versions and variants of Humanoid environment. Here, we compare between the recently adopted and potentially more challenging Humanoid-v4 environment for comparisons. Humanoid-v5 environment wasn’t used in this work because there is a lack of published contemporary models that are successfully tested on the most recent version. To build the hDQNN model for Humanoid-v4, we structured the PQC follows. The PQC is composed of $N = 10$ qubits and $M = 10$ layers quantum operations. For the

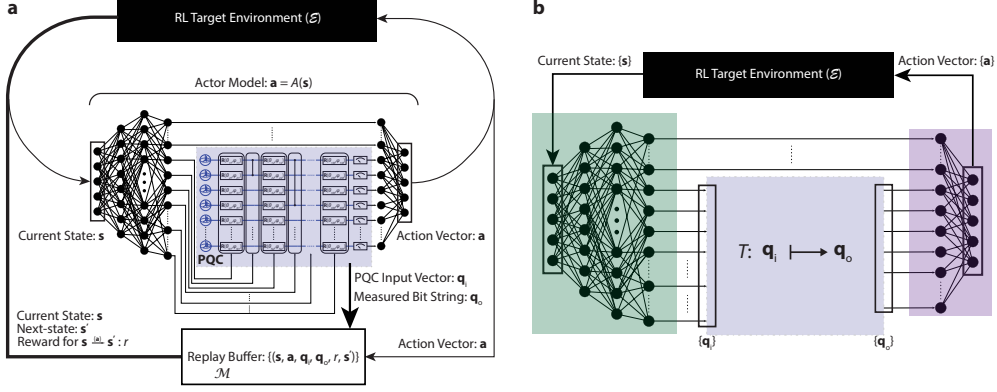


Fig. 2 **a**, the typical exploration flow for the Agent to interact with the reinforcement learning objective's target environment, \mathcal{E} , and obtain experience data to be stored in the replay buffer, \mathcal{M} . **b**, the particular modular model architecture used for the Actor Model, A , that allows the intermediate mapping T that maps its input vector \mathbf{q}_i to \mathbf{q}_o to be implemented as 1) PQC, 2) a fully connected layer, 3) uniform binary number generator, and 4) constant $\mathbf{0}$ output, without changing the rest of the model design. This offers a common testbench to compare learning performance of different representative approaches.

j -th layer, there is, first, a group of parametrized single qubit rotations where the i -th qubit in the layer is rotated by the rotation operator $\mathbf{R}(\theta_{ij}, \phi_{ij})$ with rotation angles provided by $2N$ output neurons of PreDNN. Following the single qubit rotations in the j -th layer, there is also an entanglement step that carries out one CZ-gate between p_j -th and k_j -th qubits for $p_j \neq k_j$, or reduces to identity when $p_j = k_j$, where p_j and k_j are produced by rounding two output neurons' values of PreDNN. There are in total $(2N + 2)M$ output neurons of PreDNN for controlling the PQC directly. The PQC's initial state is fixed to $|0\rangle^{\otimes N}$ and input data is encoded in the controlling parameters. $\{\theta_{ij}, \phi_{ij}, p_j, k_j\}$.

For solving RL with machine learning techniques, we can similarly identify the four processes in training: exploration, forward, backward, and update. RL problems are typically defined by its environment \mathcal{E} . An environment is fully characterized by its current state \mathbf{s} and its response to an external action vector \mathbf{a} at this current state. The \mathcal{E} responds to \mathbf{a} conditioned on being in \mathbf{s} are the new state \mathbf{s}' of \mathcal{E} caused by \mathbf{a} and a scalar reward value, r , for $\mathbf{s} \xrightarrow{\mathbf{a}} \mathbf{s}'$.

Utilizing DNNs to solve an RL problem typically requires training two models together as illustrated in Fig. 3. One is the Actor Model, $A(\mathbf{s}) \rightarrow \mathbf{a}$, which suggests an action vector, \mathbf{a} , for a given observed current environment state, \mathbf{s} , to maximize the total reward, $R = \sum r$, over its future interactions with the \mathcal{E} from current state, \mathbf{s} . As the \mathcal{E} is generally not analytically predictable or even deterministic, another useful DNN-based model is the Critic Model, $C(\mathbf{s}, \mathbf{a}) \rightarrow R$. This model aims to self-consistently approximate the maximal total reward of an action \mathbf{a} for a given environment state \mathbf{s} . As the Actor Model drives real actions when the trained RL model is applied to real-world open-loop problems, a more generalizable Actor Model will directly impact the real-world tasks. Therefore, we first start by building the Actor Model based on hDQNN and keep the Critical Model purely classical.

Algorithm 1: Training an hDQNN with qtDNN for Reinforcement Learning

Input:

Environment \mathcal{E} with states s , actions a , and rewards r ;
Discount factor γ ; maximum training iterations N_{step} ;
Actor model A (with a Quantum Layer QL, preDNN, and postDNN); Critic model C ;
following the practice of TD3, there are two Critic Models to stabilize training.
Target (delayed) Critic model C_t and Actor model A_t ; replay buffer \mathcal{M} ;
Neural local approximator of QL for each sampled training data batch qtDNN;
Learning rates for Actor (preDNN and postDNN), Critic, and qtDNN (α_A , α_C , α_{qt});
qtDNN training times N_{qt} and Actor update delays N_A for each model update epoch.

for iteration = 1 to N_{step} **do**

(A) *Exploration / Data Collection:*

1. Observe current state \mathbf{s} from \mathcal{E} .
2. Compute action $\mathbf{a} = A(\mathbf{s})$, which includes:
 - (a) Forward pass through Actor's classical layers (PreDNN) and get \mathbf{q}_i .
 - (b) Evaluate quantum layer QL on input \mathbf{q}_i to sample out \mathbf{q}_o .
 - (c) Pass \mathbf{q}_o and d_{c-link} connections from preDNN to PostDNN to predict action \mathbf{a} .
Gaussian exploration noise is added to \mathbf{a}
3. Apply \mathbf{a} in environment \mathcal{E} , observe reward r and next state \mathbf{s}' .
4. Store transition $(\mathbf{s}, \mathbf{a}, \mathbf{q}_i, \mathbf{q}_o, r, \mathbf{s}')$ in replay buffer \mathcal{M} .

(B) *Update DNNs:*

Sample a batch \mathcal{B} containing N_b entries of $(\mathbf{s}, \mathbf{a}, \mathbf{q}_i, \mathbf{q}_o, r, \mathbf{s}')$ from \mathcal{M}

(B1) *Tangential Network (qtDNN) Update:*

1. Sample N_{qt} tiny-batches $\{\mathcal{B}_{qt}\}$ from \mathcal{B} containing $\{(\mathbf{q}_i, \mathbf{q}_o)\}$.
2. **for** \mathcal{B}_{qt} in $\{\mathcal{B}_{qt}\}$ **do**
 Update qtDNN's parameters θ_{qt} (with learning rate α_{qt}) by minimizing
 BCELoss(qtDNN(\mathbf{q}_i), \mathbf{q}_o) for \mathcal{B}_{qt} .
end for

(B2) *Critic Update:*

1. For each sample, compute next-action $\mathbf{a}_t = A_{t,qt}(\mathbf{s}')$,
 where $A_{t,qt}$ is the surrogate target Actor A_t
2. Compute Critic target:
 $R_t = r + \gamma C_t(\mathbf{s}', \hat{\mathbf{a}})$.
3. Update C 's parameters θ_C by minimizing the TD-loss $\|C(\mathbf{s}, \mathbf{a}) - R_t\|$.

(B3) *Actor Update (via qtDNN) if iteration mod N_A is 0 :*

1. Compute actions $\hat{\mathbf{a}} = A_{qt}(\mathbf{s})$ for each \mathbf{s} .
 where A_{qt} is the Actor A with the quantum layer replaced by qtDNN.
2. Update Actor's classical parameters, θ_A by *maximizing* Critic's value:
 $R = C(\mathbf{s}, A_{qt}(\mathbf{s}))$
 via standard backprop through qtDNN instead of QL.

(B4) *Target Critic Update if iteration mod N_A is 0 :*

- Soft update $\theta_{C_t} \leftarrow \tau \theta_C + (1 - \tau) \theta_{C_t}$, where $0 < \tau < 1$.
Soft update $\theta_{A_t} \leftarrow \tau \theta_A + (1 - \tau) \theta_{A_t}$, where $0 < \tau < 1$.

end for

Output: Final trained Actor A (with quantum layer QL) and Critic C .

Table 1 Pseudocode for training a hybrid Deep Quantum Neural Network (hDQNN) with qtDNN-based tangential approximation in a reinforcement learning setting.

In the exploration process shown in in Fig. 2, the \mathbf{s} is observed as an input into the hDQNN-based Actor Model. The input passes through the Actor Model’s classical DNNs and quantum layers toward suggesting an action vector \mathbf{a} as its output. \mathbf{a} is then applied to the classical environment \mathcal{E} , which transitions to a new state \mathbf{s}' with a scalar reward r . Similar to conventional RL frameworks, we introduce a replay buffer (\mathcal{M}) that stores each environment transition together corresponding quantum layers’ input \mathbf{q}_i and output \mathbf{q}_o , $(\mathbf{s}, \mathbf{a}, \mathbf{q}_i, \mathbf{q}_o, r, \mathbf{s}')$, as an element.

After the exploration process that generates sufficient data entries in the \mathcal{M} , we could then sample a number (N_b) of entries randomly from the \mathcal{M} as a batch. As seen in Fig. 3, Elements corresponding to quantum layers’ \mathbf{q}_i and \mathbf{q}_o in the batched entries are extracted to train and update qtDNNs approximating quantum layers of the Actor Model to the first order within the data.

After updating qtDNNs and obtaining an updated surrogate Actor Model A_{qt} with qtDNNs replacing PQCs of A as batch training compatible moving local approximation for quantum layers, we train and update the classical Critic Model using the standard Temporal Difference (TD) learning method. For training C (A) we define a target network C_t (A_t), which is a time-delayed copy of C (A). Similarly, we also define surrogate target network $A_{t,qt}$ from A_{qt} with its PQCs similarly replaced with qtDNNs. We calculate the estimated total reward using two methods. These two methods should converge on the final values as the training for C converges. Therefore, we train the prediction of C consistently in the iterative training rounds. One method is straightforward, using the batched sampled values for \mathbf{s} and \mathbf{a} to predict total reward $R = C(\mathbf{s}, \mathbf{a})$. The other method tries to predict the same value using the fact that total reward could also be calculated as $R_t = r + C_t(\mathbf{s}', A_{t,qt}(\mathbf{s}'))$ if the training for $C \simeq C_t$ converges to accurately predicting the total reward $R \simeq R_t$ and $A \simeq A_{qt}$ also suggests approximately optimal \mathbf{a} that lead to the largest total future reward from \mathbf{s} . Training C is to update its parameters such that it minimizes the loss function characterizing the difference between R and R_t . Note that it is only necessary to backpropagate errors through C and update its parameters this way. C_t is updated by copying slightly older parameters of C to keep a time delay between them to avoid oscillatory feedback behaviors causing instability in training. A is only updated through batched backpropagation in the following step.

Now, we have updated C and the qtDNNs of A_{qt} with the classical DNNs shared with A unchanged. In the last step, we train and update the classical DNNs of A (A_{qt}) using the qtDNNs as an approximation for the quantum layers to the first order in the batched training. We forward pass batched \mathbf{s} into A_{qt} and C for getting the batched predicted optimal total reward, $R = C(\mathbf{s}, A_{qt}(\mathbf{s}))$. The parameters of only the classical DNNs of A (A_{qt}) are updated to maximize the R using batched backpropagation through C and A_{qt} .

In the rest of this section, we show an experiment implementing qtDNN-based QRL for solving the Humanoid-v4 environment provided by the standard Gymnasium library [13]. We constructed the model in this experiment by modifying Twin Delayed DDPG (TD3) [16, 20]. Allowing for a direct comparison between quantum and classical alternatives based on the same TD3 architecture, we constructed the Actor model as

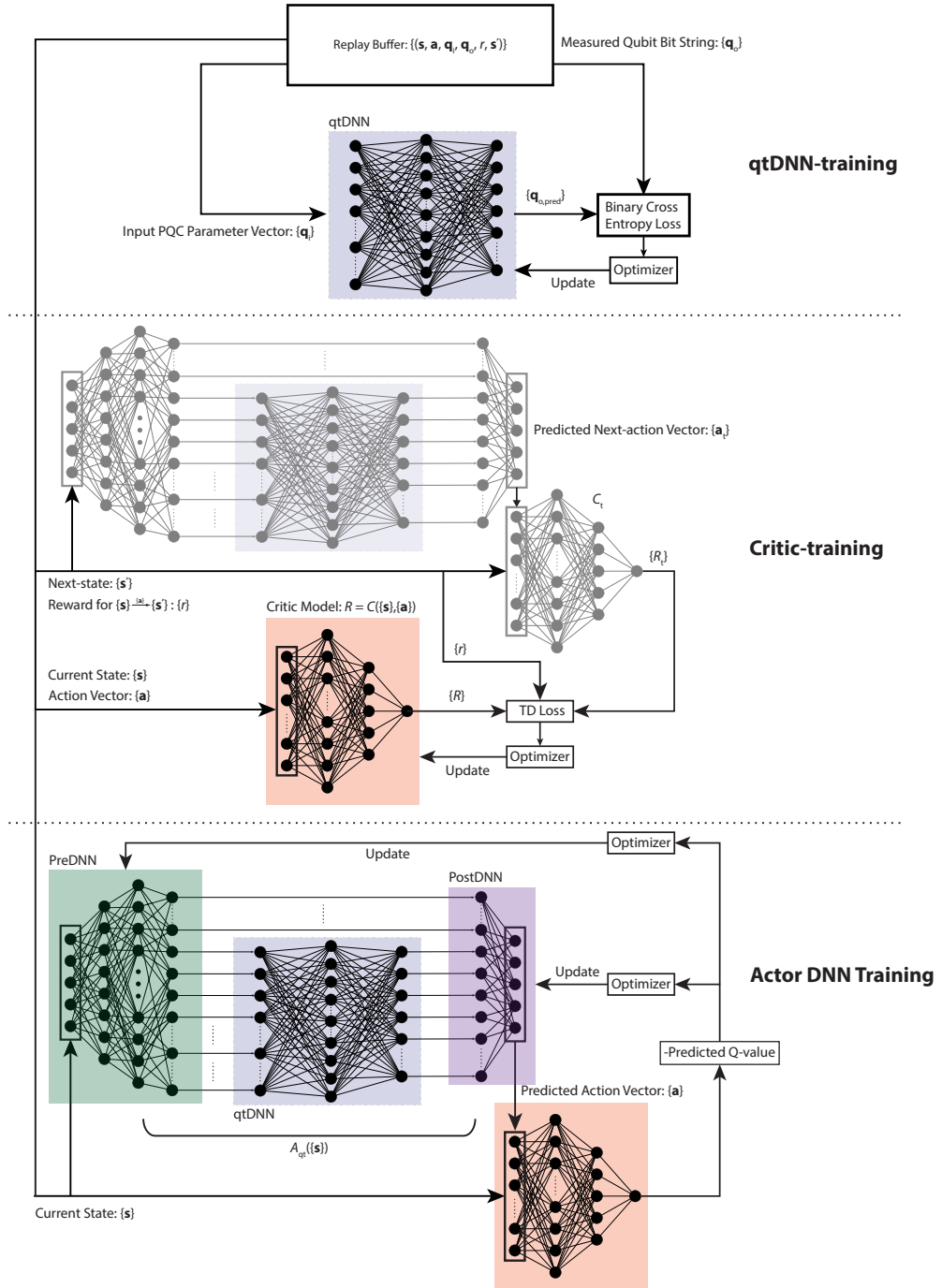


Fig. 3 The batched training process flow that incorporates qtDNN training framework for efficiently updating the classical neural layers of the hDQNN model to achieve desired learning goals.

shown in Fig. 2a-b and kept the Critic model purely classical. The classical parts of Actor and Critic models are designed and trained with the parameters in Table 2.

In this experiment, as illustrated in Fig. 2b, the Actor model has a generic block $T : \mathbf{q}_i \rightarrow \mathbf{q}_o$ with input vector \mathbf{q}_i and output vector \mathbf{q}_o . Different model constructions are compared by implementing the block with appropriate mapping mechanisms from the input to the output. For this experiment, we implemented the block as 1) PQC, 2) fully-connected linear map (FC), 3) uniform random binary generator (RBG), and 4) constant zeros (0L).

The trained hDQNN-based Actor model outperforms the classical models in terms of test rewards, demonstrating a potential advantage in generalizability. The learning process with key indicators is shown in Fig. 4. We noticed that both FC and 0L models underperformed PQC and FC models by a large margin in test rewards with the same exploration noise. This observation is further contrasted with the high rewards achieved in the training loop. It highlights entropy’s role in encouraging the model to be trained towards a generalizable global optimal in reinforcement learning for complex environments [5, 6]. On the other hand, hDQNN-based model outperforms RBG-based model. It further indicates that learning a structured randomness towards the complex correlated dynamics of a complex high-dimensional environment is desired as learning decreases model entropy [5, 6] for gaining information from interacting with a previously unknown environment. We note that a simple experiment was done for the Pendulum-v1 environment provided by the standard Gymnasium library. The environment is significantly simpler with only a three-dimensional observation space and a one-dimensional action space. The results show that hDQNN-based Actor model trained with qtDNN framework performed optimally with saturating scores on par with alternatives. However, in this simpler environment, we observed that RBG-based model underperformed both quantum and classical alternatives (FC and 0L). The result further highlights that even though entropy encourages generalizability in reinforcement learning [6], unstructured randomness that can’t be trained to decrease entropy for the environment to be encoded into the model hinders learning efficiently, especially for simpler and deterministic environments.

4 Discussion

Comparing the hDQNN trained with the qtDNN framework with alternative classical models, we observed novel behaviors that could provide insights into the fundamental dynamics and physics in learning. These insights could be useful for implementing future improvements and applying the hDQNN+qtDNN framework to major machine learning problems including training and inferences related to the frontier large language models (LLMs) and advanced robotics.

In the experiments to understand hDQNN’s abilities to learn a complex environment’s dynamics efficiently, we implemented a hDQNN reinforcement learning model where its PQC layer could be swapped to alternative classical mappings. This offers a direct way to compare PQC and classical alternatives with other variables kept the same. This work demonstrated hDQNN’s potential generalizability advantage in quantum reinforcement learning over classical counterparts including public models

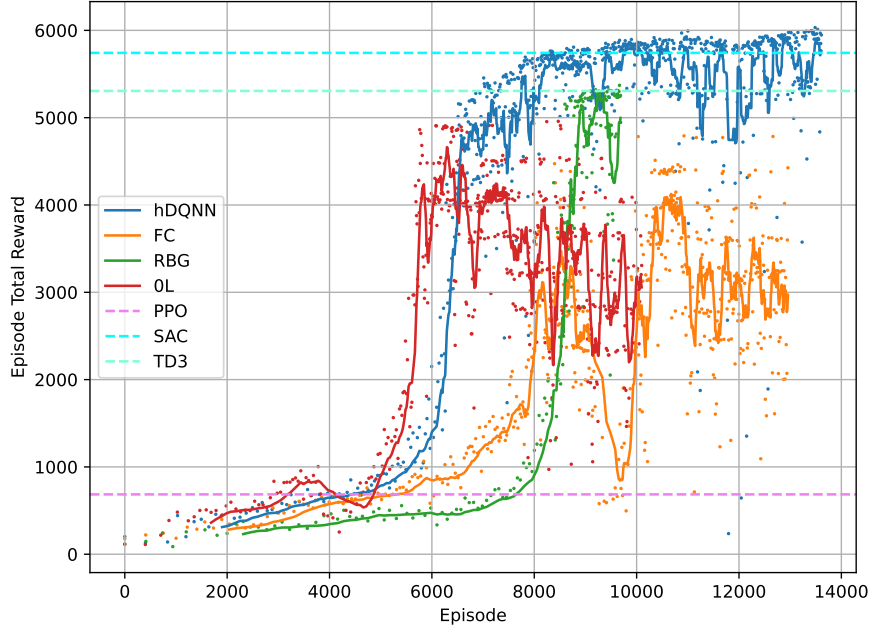


Fig. 4 The total test reward for the trained agents to control the humanoid to walk in Humanoid-v4 environment. The solid lines are rolling window smooth over 10 test rounds. Each test round has 10 testing episode and each round’s averaged episode reward is shown as dots in the plot. As the tests are carried out periodically during the training, the horizontal axis records the training episode after which the round of tests is carried out. The dashed lines correspond to performance of classical RL models implemented with widely used SOTA architectures [17–19].

implemented with SOTA architectures. To the best of our knowledge, this is also the first time quantum machine learning has been applied successfully to a complex high-dimensional reinforcement learning task like the Humanoid-v4, which could potentially be applied in advanced robotics.

In this work, we have provided a novel architecture for efficiently training hDQNN for practical, complicated ML tasks. We further applied this architecture to reinforcement learning and benchmark its performance in the complex high-dimensional Humanoid-v4 environment against classical alternatives. The improved generalizability, shown through achieving the highest test episode rewards (see Fig. 4), of hDQNN model trained with qtDNN highlights the importance of learning stochastic correlations and optimizing entropy in challenging reinforcement learning tasks. In principle, modeling of complicated classical correlated stochastic behaviors in a classical environment could be learned purely through classical models, and there might indeed be classical models inspired by this work to solve specific reinforcement learning tasks. The merit of hDQNNs trained with qtDNN is that hDQNNs have a higher degree of

Table 2 hDQNN Reinforcement Learning Model Configuration for Gymnasium Humanoid-v4 Problem

Components	DNN Design ¹		Hyperparameters ²				
	Layers	Activation	N^3, M^4	d_{c-link}^5	α^6	γ^7	τ^8
PreDNN	[376,256,230]	Leaky Relu	10,10	10	$3e^{-4}$		$5e^{-3}$
qtDNN	[220,2048,10]	Leaky Relu			$3e^{-4}$		
PQC							
PostDNN	[20,256,17]	Leaky Relu		10	$3e^{-4}$		$5e^{-3}$
Critic	[[376,256],[273,256,1]] ⁹	Leaky Relu			$3e^{-4}$	0.99	$5e^{-3}$

Note: Other TD3 parameters such as the exploration action policy noises follow <https://huggingface.co/sdpkjc/Humanoid-v4-td3-continuous-action-seed5>

¹DNN designs shared between comparable alternatives

²Hyperparameters shared between comparable alternatives

³The number of qubits in PQC

⁴The number of layers in PQC

⁵The number of classical links directly between PreDNN and PostDNN

⁶Learning rate

⁷The reward discount parameter

⁸Soft target model update rate

⁹The Critic Model has two segments similar to [20] and this represents the configuration of the two segments in forward direction.

expressivity, while being straightforward for (noisy) hybrid quantum classical hardware to execute hDQNN in runtime, could model correlated stochastic processes that are hard for classical models to simulate [8] with comparable classical resources. Training hDQNN+qtDNN and inferencing with hDQNN on (noisy) quantum hardware offer a new route in reinforcement learning and AI research for addressing complicated real-world problems that are always stochastic, highly correlated, and even challenging to describe with low computing complexities.

References

- [1] Wang, Y., Liu, J.: A comprehensive review of quantum machine learning: from nisq to fault tolerance. Reports on Progress in Physics **87**(11), 116402 (2024) <https://doi.org/10.1088/1361-6633/ad7f69>
- [2] Robison, K.: OpenAI cofounder Ilya Sutskever says the way AI is built is about to change (2024). <https://www.theverge.com/2024/12/13/24320811/what-ilya-sutskever-sees-openai-model-data-training>
- [3] Harrow, A.W., Hassidim, A., Lloyd, S.: Quantum algorithm for linear systems of equations. PRL **103**(15), 150502 (2009) <https://doi.org/10.1103/PhysRevLett.103.150502>

- [4] ACM: Acm a.m. turing award honors two researchers who led the development of cornerstone ai technology (2025). Accessed: 2025-03-05
- [5] Schulman, J., Wolski, F., Dhariwal, P., Radford, A., Klimov, O.: Proximal policy optimization algorithms (2017) [arXiv:1707.06347](#) [cs.LG]
- [6] Haarnoja, T., Zhou, A., Abbeel, P., Levine, S.: Soft actor-critic: Off-policy maximum entropy deep reinforcement learning with a stochastic actor (2018) [arXiv:1801.01290](#) [cs.LG]
- [7] DeepSeek-AI, Guo, D., Yang, D., Zhang, H., Song, J., Zhang, R., Xu, R., Zhu, Q., Ma, S., Wang, P., Bi, X., Zhang, X., Yu, X., Wu, Y., Wu, Z.F., Gou, Z., Shao, Z., Li, Z., Gao, Z., Liu, A., Xue, B., Wang, B., Wu, B., Feng, B., Lu, C., Zhao, C., Deng, C., Zhang, C., Ruan, C., Dai, D., Chen, D., Ji, D., Li, E., Lin, F., Dai, F., Luo, F., Hao, G., Chen, G., Li, G., Zhang, H., Bao, H., Xu, H., Wang, H., Ding, H., Xin, H., Gao, H., Qu, H., Li, H., Guo, J., Li, J., Wang, J., Chen, J., Yuan, J., Qiu, J., Li, J., Cai, J.L., Ni, J., Liang, J., Chen, J., Dong, K., Hu, K., Gao, K., Guan, K., Huang, K., Yu, K., Wang, L., Zhang, L., Zhao, L., Wang, L., Zhang, L., Xu, L., Xia, L., Zhang, M., Zhang, M., Tang, M., Li, M., Wang, M., Li, M., Tian, N., Huang, P., Zhang, P., Wang, Q., Chen, Q., Du, Q., Ge, R., Zhang, R., Pan, R., Wang, R., Chen, R.J., Jin, R.L., Chen, R., Lu, S., Zhou, S., Chen, S., Ye, S., Wang, S., Yu, S., Zhou, S., Pan, S., Li, S.S., Zhou, S., Wu, S., Ye, S., Yun, T., Pei, T., Sun, T., Wang, T., Zeng, W., Zhao, W., Liu, W., Liang, W., Gao, W., Yu, W., Zhang, W., Xiao, W.L., An, W., Liu, X., Wang, X., Chen, X., Nie, X., Cheng, X., Liu, X., Xie, X., Liu, X., Yang, X., Li, X., Su, X., Lin, X., Li, X.Q., Jin, X., Shen, X., Chen, X., Sun, X., Wang, X., Song, X., Zhou, X., Wang, X., Shan, X., Li, Y.K., Wang, Y.Q., Wei, Y.X., Zhang, Y., Xu, Y., Li, Y., Zhao, Y., Sun, Y., Wang, Y., Yu, Y., Zhang, Y., Shi, Y., Xiong, Y., He, Y., Piao, Y., Wang, Y., Tan, Y., Ma, Y., Liu, Y., Guo, Y., Ou, Y., Wang, Y., Gong, Y., Zou, Y., He, Y., Xiong, Y., Luo, Y., You, Y., Liu, Y., Zhou, Y., Zhu, Y.X., Xu, Y., Huang, Y., Li, Y., Zheng, Y., Zhu, Y., Ma, Y., Tang, Y., Zha, Y., Yan, Y., Ren, Z.Z., Ren, Z., Sha, Z., Fu, Z., Xu, Z., Xie, Z., Zhang, Z., Hao, Z., Ma, Z., Yan, Z., Wu, Z., Gu, Z., Zhu, Z., Liu, Z., Li, Z., Xie, Z., Song, Z., Pan, Z., Huang, Z., Xu, Z., Zhang, Z., Zhang, Z.: Deepseek-r1: Incentivizing reasoning capability in llms via reinforcement learning (2025) [arXiv:2501.12948](#) [cs.CL]
- [8] Arute, F., Arya, K., Babbush, R., Bacon, D., Bardin, J.C., Barends, R., Biswas, R., Boixo, S., Brandao, F.G.S.L., Buell, D.A., Burkett, B., Chen, Y., Chen, Z., Chiaro, B., Collins, R., Courtney, W., Dunsworth, A., Farhi, E., Foxen, B., Fowler, A., Gidney, C., Giustina, M., Graff, R., Guerin, K., Habegger, S., Harrigan, M.P., Hartmann, M.J., Ho, A., Hoffmann, M., Huang, T., Humble, T.S., Isakov, S.V., Jeffrey, E., Jiang, Z., Kafri, D., Kechedzhi, K., Kelly, J., Klimov, P.V., Knysh, S., Korotkov, A., Kostritsa, F., Landhuis, D., Lindmark, M., Lucero, E., Lyakh, D., Mandrà, S., McClean, J.R., McEwen, M., Megrant, A., Mi, X., Michielsen, K., Mohseni, M., Mutus, J., Naaman, O., Neeley, M.,

Neill, C., Niu, M.Y., Ostby, E., Petukhov, A., Platt, J.C., Quintana, C., Riefel, E.G., Roushan, P., Rubin, N.C., Sank, D., Satzinger, K.J., Smelyanskiy, V., Sung, K.J., Trevithick, M.D., Vainsencher, A., Villalonga, B., White, T., Yao, Z.J., Yeh, P., Zalcman, A., Neven, H., Martinis, J.M.: Quantum supremacy using a programmable superconducting processor. *Nature* **574**(7779), 505–510 (2019) <https://doi.org/10.1038/s41586-019-1666-5>

- [9] Acharya, R., Abanin, D.A., Aghababaie-Beni, L., Aleiner, I., Andersen, T.I., Ansmann, M., Arute, F., Arya, K., Asfaw, A., Astrakhantsev, N., Atalaya, J., Babbush, R., Bacon, D., Ballard, B., Bardin, J.C., Bausch, J., Bengtsson, A., Bilmes, A., Blackwell, S., Boixo, S., Bortoli, G., Bourassa, A., Bovaird, J., Brill, L., Broughton, M., Browne, D.A., Buchea, B., Buckley, B.B., Buell, D.A., Burger, T., Burkett, B., Bushnell, N., Cabrera, A., Campero, J., Chang, H.-S., Chen, Y., Chen, Z., Chiaro, B., Chik, D., Chou, C., Claes, J., Cleland, A.Y., Cogan, J., Collins, R., Conner, P., Courtney, W., Crook, A.L., Curtin, B., Das, S., Davies, A., De Lorenzo, L., Debroy, D.M., Demura, S., Devoret, M., Di Paolo, A., Donohoe, P., Drozdov, I., Dunsworth, A., Earle, C., Edlich, T., Eickbusch, A., Elbag, A.M., Elzouka, M., Erickson, C., Faoro, L., Farhi, E., Ferreira, V.S., Burgos, L.F., Forati, E., Fowler, A.G., Foxen, B., Ganjam, S., Garcia, G., Gasca, R., Genois, E., Giang, W., Gidney, C., Gilboa, D., Gosula, R., Dau, A.G., Graumann, D., Greene, A., Gross, J.A., Habegger, S., Hall, J., Hamilton, M.C., Hansen, M., Harrigan, M.P., Harrington, S.D., Heras, F.J.H., Heslin, S., Heu, P., Higgott, O., Hill, G., Hilton, J., Holland, G., Hong, S., Huang, H.-Y., Huff, A., Huggins, W.J., Ioffe, L.B., Isakov, S.V., Iveland, J., Jeffrey, E., Jiang, Z., Jones, C., Jordan, S., Joshi, C., Juhas, P., Kafri, D., Kang, H., Karamlou, A.H., Kechedzhi, K., Kelly, J., Khaire, T., Khattar, T., Khezri, M., Kim, S., Klimov, P.V., Klots, A.R., Kobrin, B., Kohli, P., Korotkov, A.N., Kostitsa, F., Kothari, R., Kozlovskii, B., Kreikebaum, J.M., Kurilovich, V.D., Lacroix, N., Landhuis, D., Lange-Dei, T., Langley, B.W., Laptev, P., Lau, K.-M., Le Guevel, L., Ledford, J., Lee, J., Lee, K., Lensky, Y.D., Leon, S., Lester, B.J., Li, W.Y., Li, Y., Lill, A.T., Liu, W., Livingston, W.P., Locharla, A., Lucero, E., Lundahl, D., Lunt, A., Madhuk, S., Malone, F.D., Maloney, A., Mandrà, S., Manyika, J., Martin, L.S., Martin, O., Martin, S., Maxfield, C., McClean, J.R., McEwen, M., Meeks, S., Megrant, A., Mi, X., Miao, K.C., Mieszala, A., Molavi, R., Molina, S., Montazeri, S., Morvan, A., Movasagh, R., Mruczkiewicz, W., Naaman, O., Neeley, M., Neill, C., Nersisyan, A., Neven, H., Newman, M., Ng, J.H., Nguyen, A., Nguyen, M., Ni, C.-H., Niu, M.Y., O’Brien, T.E., Oliver, W.D., Opremcak, A., Ottosson, K., Petukhov, A., Pizzuto, A., Platt, J., Potter, R., Pritchard, O., Pryadko, L.P., Quintana, C., Ramachandran, G., Reagor, M.J., Redding, J., Rhodes, D.M., Roberts, G., Rosenberg, E., Rosenfeld, E., Roushan, P., Rubin, N.C., Saei, N., Sank, D., Sankaragomathi, K., Satzinger, K.J., Schurkus, H.F., Schuster, C., Senior, A.W., Shearn, M.J., Shorter, A., Shutty, N., Shvarts, V., Singh, S., Sivak, V., Skrzynny, J., Small, S., Smelyanskiy, V., Smith, W.C., Somma, R.D., Springer, S., Sterling, G., Strain, D., Suchard, J., Szasz, A., Szein, A., Thor, D., Torres, A., Torunbalci, M.M., Vaishnav, A., Vargas, J., Vdovichev, S., Vidal, G., Villalonga, B., Heidweiller, C.V., Waltman, S., Wang, S.X., Ware, B., Weber, K., Weidel, T., White, T.,

- Wong, K., Woo, B.W.K., Xing, C., Yao, Z.J., Yeh, P., Ying, B., Yoo, J., Yosri, N., Young, G., Zalcman, A., Zhang, Y., Zhu, N., Zobrist, N., Google Quantum, A.I., Collaborators: Quantum error correction below the surface code threshold. *Nature* **638**(8052), 920–926 (2025) <https://doi.org/10.1038/s41586-024-08449-y>
- [10] Gao, D., Fan, D., Zha, C., Bei, J., Cai, G., Cai, J., Cao, S., Chen, F., Chen, J., Chen, K., Chen, X., Chen, X., Chen, Z., Chen, Z., Chen, Z., Chu, W., Deng, H., Deng, Z., Ding, P., Ding, X., Ding, Z., Dong, S., Dong, Y., Fan, B., Fu, Y., Gao, S., Ge, L., Gong, M., Gui, J., Guo, C., Guo, S., Guo, X., Han, L., He, T., Hong, L., Hu, Y., Huang, H.-L., Huo, Y.-H., Jiang, T., Jiang, Z., Jin, H., Leng, Y., Li, D., Li, D., Li, F., Li, J., Li, J., Li, J., Li, J., Li, N., Li, S., Li, W., Li, Y., Li, Y., Liang, F., Liang, X., Liao, N., Lin, J., Lin, W., Liu, D., Liu, H., Liu, M., Liu, X., Liu, X., Liu, Y., Lou, H., Ma, Y., Meng, L., Mou, H., Nan, K., Nie, B., Nie, M., Ning, J., Niu, L., Peng, W., Qian, H., Rong, H., Rong, T., Shen, H., Shen, Q., Su, H., Su, F., Sun, C., Sun, L., Sun, T., Sun, Y., Tan, Y., Tan, J., Tang, L., Tu, W., Wan, C., Wang, J., Wang, B., Wang, C., Wang, C., Wang, C., Wang, J., Wang, L., Wang, R., Wang, S., Wang, X., Wang, X., Wang, X., Wang, Y., Wei, Z., Wei, J., Wu, D., Wu, G., Wu, J., Wu, S., Wu, Y., Xie, S., Xin, L., Xu, Y., Xue, C., Yan, K., Yang, W., Yang, X., Yang, Y., Ye, Y., Ye, Z., Ying, C., Yu, J., Yu, Q., Yu, W., Zeng, X., Zhan, S., Zhang, F., Zhang, H., Zhang, K., Zhang, P., Zhang, W., Zhang, Y., Zhang, Y., Zhang, L., Zhao, G., Zhao, P., Zhao, X., Zhao, X., Zhao, Y., Zhao, Z., Zheng, L., Zhou, F., Zhou, L., Zhou, N., Zhou, N., Zhou, S., Zhou, S., Zhou, Z., Zhu, C., Zhu, Q., Zou, G., Zou, H., Zhang, Q., Lu, C.-Y., Peng, C.-Z., Zhu, X., Pan, J.-W.: Establishing a new benchmark in quantum computational advantage with 105-qubit zuchongzhi 3.0 processor. *PRL* **134**(9), 090601 (2025) <https://doi.org/10.1103/PhysRevLett.134.090601>
- [11] Jin, Y.-X., Wang, Z.-W., Xu, H.-Z., Zhuang, W.-F., Hu, M.-J., Liu, D.E.: Ppo-q: Proximal policy optimization with parametrized quantum policies or values (2025) [arXiv:2501.07085](https://arxiv.org/abs/2501.07085) [quant-ph]
- [12] Raffin, A.: RL Baselines3 Zoo. GitHub (2020)
- [13] Towers, M., Kwiatkowski, A., Terry, J., Balis, J.U., De Cola, G., Deleu, T., Goulão, M., Kallinteris, A., Krimmel, M., KG, A., et al.: Gymnasium: A standard interface for reinforcement learning environments. *arXiv preprint arXiv:2407.17032* (2024)
- [14] Vaswani, A., Shazeer, N., Parmar, N., Uszkoreit, J., Jones, L., Gomez, A.N., Kaiser, L., Polosukhin, I.: Attention is all you need (2023) [arXiv:1706.03762](https://arxiv.org/abs/1706.03762) [cs.CL]
- [15] DeepSeek-AI, Liu, A., Feng, B., Xue, B., Wang, B., Wu, B., Lu, C., Zhao, C., Deng, C., Zhang, C., Ruan, C., Dai, D., Guo, D., Yang, D., Chen, D., Ji, D., Li, E., Lin, F., Dai, F., Luo, F., Hao, G., Chen, G., Li, G., Zhang, H., Bao, H., Xu, H., Wang, H., Zhang, H., Ding, H., Xin, H., Gao, H., Li, H., Qu, H., Cai, J.L.,

- Liang, J., Guo, J., Ni, J., Li, J., Wang, J., Chen, J., Chen, J., Yuan, J., Qiu, J., Li, J., Song, J., Dong, K., Hu, K., Gao, K., Guan, K., Huang, K., Yu, K., Wang, L., Zhang, L., Xu, L., Xia, L., Zhao, L., Wang, L., Zhang, L., Li, M., Wang, M., Zhang, M., Zhang, M., Tang, M., Li, M., Tian, N., Huang, P., Wang, P., Zhang, P., Wang, Q., Zhu, Q., Chen, Q., Du, Q., Chen, R.J., Jin, R.L., Ge, R., Zhang, R., Pan, R., Wang, R., Xu, R., Zhang, R., Chen, R., Li, S.S., Lu, S., Zhou, S., Chen, S., Wu, S., Ye, S., Ye, S., Ma, S., Wang, S., Zhou, S., Yu, S., Zhou, S., Pan, S., Wang, T., Yun, T., Pei, T., Sun, T., Xiao, W.L., Zeng, W., Zhao, W., An, W., Liu, W., Liang, W., Gao, W., Yu, W., Zhang, W., Li, X.Q., Jin, X., Wang, X., Bi, X., Liu, X., Wang, X., Shen, X., Chen, X., Zhang, X., Chen, X., Nie, X., Sun, X., Wang, X., Cheng, X., Liu, X., Xie, X., Liu, X., Yu, X., Song, X., Shan, X., Zhou, X., Yang, X., Li, X., Su, X., Lin, X., Li, Y.K., Wang, Y.Q., Wei, Y.X., Zhu, Y.X., Zhang, Y., Xu, Y., Xu, Y., Huang, Y., Li, Y., Zhao, Y., Sun, Y., Li, Y., Wang, Y., Yu, Y., Zheng, Y., Zhang, Y., Shi, Y., Xiong, Y., He, Y., Tang, Y., Piao, Y., Wang, Y., Tan, Y., Ma, Y., Liu, Y., Guo, Y., Wu, Y., Ou, Y., Zhu, Y., Wang, Y., Gong, Y., Zou, Y., He, Y., Zha, Y., Xiong, Y., Ma, Y., Yan, Y., Luo, Y., You, Y., Liu, Y., Zhou, Y., Wu, Z.F., Ren, Z.Z., Ren, Z., Sha, Z., Fu, Z., Xu, Z., Huang, Z., Zhang, Z., Xie, Z., Zhang, Z., Hao, Z., Gou, Z., Ma, Z., Yan, Z., Shao, Z., Xu, Z., Wu, Z., Zhang, Z., Li, Z., Gu, Z., Zhu, Z., Liu, Z., Li, Z., Xie, Z., Song, Z., Gao, Z., Pan, Z.: Deepseek-v3 technical report (2025) [arXiv:2412.19437](https://arxiv.org/abs/2412.19437) [cs.CL]
- [16] Fujimoto, S., Hoof, H., Meger, D.: Addressing function approximation error in actor-critic methods (2018) [arXiv:1802.09477](https://arxiv.org/abs/1802.09477) [cs.AI]
- [17] sdpkjc: Humanoid v4 ppo fix continuous action seed4 (2024). https://huggingface.co/sdpkjc/Humanoid-v4-ppo_fix_continuous_action-seed4
- [18] sdpkjc: Humanoid v4 sac continuous action seed5 (2023). https://huggingface.co/sdpkjc/Humanoid-v4-sac_continuous_action-seed5
- [19] sdpkjc: Humanoid v4 td3 continuous action seed3 (2023). https://huggingface.co/sdpkjc/Humanoid-v4-td3_continuous_action-seed3
- [20] Lillicrap, T.P., Hunt, J.J., Pritzel, A., Heess, N., Erez, T., Tassa, Y., Silver, D., Wierstra, D.: Continuous control with deep reinforcement learning (2019) [arXiv:1509.02971](https://arxiv.org/abs/1509.02971) [cs.LG]